Nucleon correlations and the equation of state of nuclear matter

A. Polls[*], W.H. Dickhoff[†], H. Müther[**], A. Ramos[‡], A. Rios[§] and I. Vidaña[¶]

[*]*Department d'Estructura i Constituents de la Matèria and Institut de Ciències del Cosmos, Universitat de Barcelona, Avda. Diagonal 647, E-08028 Barcelona, Spain*
[†]*Department of Physics, Washington University, St. Louis, Missouri 63130, USA*
[**]*Institut für Theoretische Physik, Universität Tübingen, D-72076 Tübingen, Germany*
[‡]*Department d'Estructura i Constituents de la Matèria and Institut de Ciències del Cosmos, Universitat de Barcelona, Avda. Daigonal 647, E-08028 Barcelona, Spain*
[§]*Department of Physics, Faculty of Engineering and Physical Sciences, University of Surrey, Guildford, Surrey GU2 7XH, United Kingdom*
[¶]*Centro de Física Computacional, Department of Physics, University of Coimbra, PT-3004-516 Coimbra, Portugal*

Abstract. The self-consistent Green's function method within the ladder approximation provides a microscopic description of correlated nuclear systems which properly treats the nucleon-nucleon correlations induced by the short-range and tensor components present in any realistic interaction. These correlations produce a sizable depletion of low momenta below the Fermi surface as well as the occupation of high momenta in the nuclear ground state. A few representative results for nuclear matter are presented to illustrate the present progress in the application of this method to nuclear systems.

Keywords: Nucleon-nucleon correlations, short-range repulsion, equation of state
PACS: 21.60.De,21.65.-f,21.65.Mn

INTRODUCTION

The microscopic description of nuclear systems in terms of the constituent nucleons interacting through realistic nucleon-nucleon interactions has been a long-standing goal in nuclear physics. The aim is to describe the static and dynamical properties of nuclear systems ranging from the deuteron to heavy nuclei and neutron stars using a single parameterization of the nuclear force. In spite of the enormous progress achieved during the last years [1] one should recognize that the nuclear many-body problem is not completely solved. Some of the difficulties are linked to the interplay between the determination of the bare nucleon-nucleon (NN) interaction and the many-body problem itself. One should therefore face two problems: the search of the NN interaction which defines the nuclear Hamiltonian and the solution of the associated Schrödinger equation, which will require sophisticated many-body methods just to find an approximate solution. In this presentation we take a couple of modern realistic interactions: the relatively soft CDBonn interaction [2] and the harder Argonne V18 (Av18) force [3] and concentrate on the search of the solution of the many-body problem.

These two interactions, describe very accurately NN scattering from the Nijmegen data base and the bound-state properties of the deuteron. In principle, all models for

realistic NN interactions incorporate the one-pion-exchange contribution and contain a phenomenological intermediate- and short-range part. Besides having a complicated operator structure, two main characteristics of these realistic interactions are the presence of a strong short-range repulsion in the central channel and the need of a tensor component to reproduce, among other things, the correct quadrupole moment of the deuteron. The fact that these interactions reproduce the same scattering data implies that the on-shell matrix elements of the NN transition scattering matrix are essentially equal. This does, however, not imply that the models for the NN interaction are identical. Moreover, the off-shell properties of each potential may be rather different. These differences can become explicitly manifest in many-body calculations. Exploring the results for different realistic interactions one can get a qualitative measure of the uncertainties associated with the bare NN interactions.

The strong short-range repulsion and tensor components present in realistic interactions produce important modifications of the nuclear wave function. These modifications can not be described within an independent particle model and are generically referred to as *correlations*. For instance, simple Hartree-Fock calculations for nuclear matter at the empirical saturation density using such realistic NN interactions provide positive energies rather than the empirical -16 MeV per nucleon.

Several theoretical approaches have been developed over the years to treat these correlations in nuclear systems, including variational techniques within the correlated basis functions [4, 5], quantum Monte Carlo [6] or more recently the Auxiliary field diffusion Monte Carlo [7]. Many efforts have been also devoted to the traditional Brueckner-Bethe-Goldstone hole-line expansion [8] in its lowest-order form, the so called Brueckner-Hartree-Fock (BHF) approximation [9]. The strong short-range repulsion prevents the use of perturbative expansions and either one incorporates explicitly the correlations in the wave function, as it is the case of the variational approaches, or performs partial summations of the perturbative series to obtain a well-behaved effective interaction. Obviously, diagrammatic notation is very helpful and gives physical insight in selecting the contributions.

The BHF approximation takes into account particle-particle correlations by solving the Bethe-Goldstone equation. Nevertheless, a minimal consistent treatment of correlations in nuclear systems requires the inclusion not only of particle-particle intermediate states but also of the hole-hole ones. The propagation of particles and holes can be treated on the same footing by means of the self-consistent Green's function (SCGF) approach [1, 10], which will be the many-body method discussed in this presentation. Great progress in the application of the SCGF method to nuclear matter has been achieved in recent years, both at zero [11] and finite temperatures [12, 13, 14, 15, 16, 17]. Here we will pay attention to finite temperature calculations. Moreover, the temperatures that we will consider are small enough to allow for conclusions for the $T = 0$ case and large enough to avoid the possibility of pairing instabilities [18].

One of the immediate consequences of the short-range repulsion of the NN interaction is that the probability to find two nucleons close to each other is substantially suppressed. This has important effects on the equation of state of nuclear matter. Moreover, these correlations affect also the one-body properties, *i.e.* high-momentum components in the many-body wave function are populated. At the same time, particle number conservation requires that these high-momentum components are to be accompanied by a

corresponding depletion of the population of states within the nuclear Fermi sea. Recent experiments at Jefferson laboratory have clarified the effects of short-range correlations on the properties of nucleons in the nuclear medium. An unambiguous signature of the presence of high-momentum nucleons was identified in an $(e,e'p)$ experiment on ^{12}C [19]. Evidence for the depletion of the states below the Fermi surface has been also provided by $(e,e'p)$ experiments on ^{208}Pb at NIKHEF in which a global depletion of around 15% of proton orbits below the Fermi energy explains the measured coincide cross sections in the missing energy and momentum domain corresponding to the mean-field single-particle states [20].

SINGLE-PARTICLE PROPERTIES

Calculations of the single-particle propagator are interesting for various reason. On the one hand, one does not need to know the full details of the nuclear wave function, but only how the system reacts when one takes out or adds a nucleon to the system. On the other, it gives access to the expected values of all single-particle operators [10].

The single-particle propagator, in the grand-canonical ensemble, is defined according to

$$iG(\mathbf{k}t,\mathbf{k}'t') = Tr\left[\hat{\rho}T[a_{\mathbf{k}}(t)a^{\dagger}_{\mathbf{k}'}(t')]\right], \tag{1}$$

where we have introduced the density matrix operator

$$\hat{\rho} = \frac{1}{Z}e^{-\beta(\hat{H}-\mu\hat{N})}, \tag{2}$$

and the partition function

$$Z = Tr\left[e^{-\beta(\hat{H}-\mu\hat{N})}\right]. \tag{3}$$

In these equations, β denotes the inverse temperature and μ is the chemical potential of the system. The symbol T stands for the time-ordering operator. Finally, the traces Tr are to be taken over all energy and particle number eigenstates of the system.

A Lehmann representation allows one to write the propagators in terms of the single-particle spectral functions

$$G(k,\omega) = \frac{1}{2\pi}\int_{-\infty}^{\infty} d\omega' \frac{A^{>}(k,\omega')}{\omega-\omega'+i\eta} + \frac{1}{2\pi}\int_{-\infty}^{\infty} d\omega' \frac{A^{<}(k,\omega')}{\omega-\omega'-i\eta}, \tag{4}$$

which are defined as:

$$A^{<}(k,\omega) = 2\pi\sum_{nm}\frac{e^{-\beta(E_m-\mu N_m)}}{Z} \mid \langle\Psi_n \mid a_k \mid \Psi_m\rangle \mid^2 \delta\left(\omega-(E_m-E_n)\right). \tag{5}$$

A similar definition holds for $A^{>}(k,\omega)$ with the use of a creation operator, $a^{\dagger}_k$. Note the presence in Eq. (5) of the thermal average on the initial states, which accounts for the thermal population of the excited states. This is different from the zero temperature case, where the ground state is considered to be the only possible initial state. The total

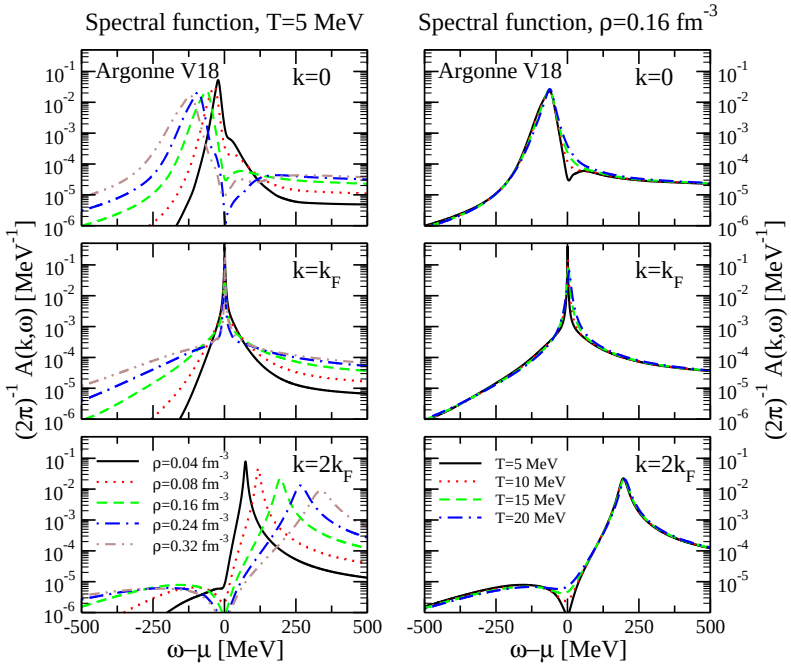

FIGURE 1. Density (left panels) and temperature (right panels) dependence of the single-particle spectral function, $A(k,\omega)$, for neutron matter, as a function of energy for three different momenta: $k=0$ (upper), $k=k_F$ (middle), and $k=2k_F$ (lower), with k_F the Fermi momentum associated with each density.

spectral function $A(k,\omega)$ is defined as the sum of the two functions, $A^<$ and $A^>$, and the following relation holds: $A^<(k,\omega)=A(k,\omega)f(\omega)$, where $f(\omega)=(1+e^{\beta(\omega-\mu)})^{-1}$ is the Fermi-Dirac distribution. The spectral functions give access to the full propagator and therefore all the single-particle properties can be obtained from $A(k,\omega)$. In particular the momentum distribution, is given by:

$$n(k)=\frac{1}{2\pi}\int_{-\infty}^{\infty}d\omega A^<(k,\omega)=\frac{1}{2\pi}\int_{-\infty}^{\infty}d\omega A(k,\omega)f(\omega)\,. \tag{6}$$

The single-particle Green's function can be obtained from the self-energy, $\Sigma(k,\omega)$, through Dyson's equation,

$$G(k,\omega)=G_0(k,\omega)\;+\;G_0(k,\omega)\Sigma(k,\omega)G(k,\omega)\,. \tag{7}$$

The self-energy accounts for the interactions of a nucleon with the nucleons in the medium and is obtained from the renormalized NN interaction in the medium. This effective interaction is calculated in the ladder approximation, propagating fully dressed particles and holes in the intermediate states of the ladder diagrams. The ladder scheme is the minimal reliable approximation to treat strong short-range repulsive interactions. By construction, the modification of the single-particle properties affects the effective interaction in the medium. Conversely, the single-particle propagator is derived from the NN interaction in the medium. Consequently, both the interaction and the propagator need to be computed in a self-consistent way.

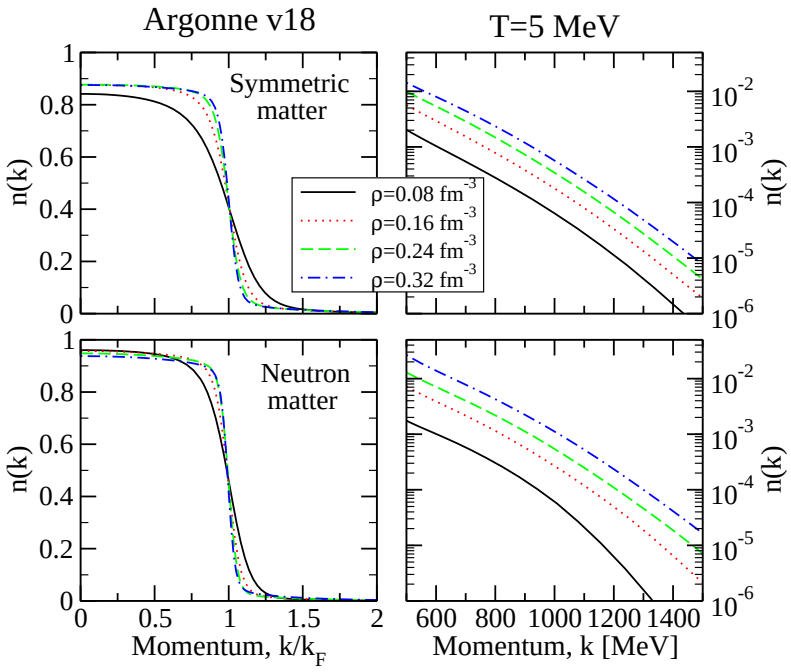

FIGURE 2. Momentum distribution of symmetric (upper panels) and neutron (lower panels) matter obtained with Av18 interaction at $T = 5$ MeV for different densities. The high momentum components are shown in the right panels.

In this procedure, the chemical potential $\bar{\mu}$ is determined by inverting:

$$\rho = \nu \int \frac{d^3k}{(2\pi)^3} n(k,\bar{\mu}) \,, \tag{8}$$

where ν denotes the spin-isospin degeneracy of the system ($\nu = 4$ and 2 in symmetric and neutron matter, respectively). Once convergence is reached, one obtains the single-particle propagator from Dyson's equation and, from its imaginary part, the spectral function $A(k,\omega)$:

$$A(k,w) = \frac{-2Im\Sigma(k,\omega)}{[\omega - \frac{\hbar^2k^2}{2m} - Re\Sigma(k,\omega)]^2 + [Im\Sigma(k,\omega)]^2} \,. \tag{9}$$

At this point, for the case of two-body interactions, one can calculate the energy per particle of the system, by means of the Galitskii-Migdal-Koltun sum rule:

$$\frac{E}{N}(\rho,T) = \frac{\nu}{\rho} \int \frac{d^3k}{(2\pi)^3} \int_{-\infty}^{\infty} \frac{d\omega}{2\pi} \frac{1}{2} \left(\frac{\hbar^2k^2}{2m} + \omega \right) A(k,\omega) f(\omega) \,. \tag{10}$$

Fig. 1 shows the density and temperature dependence of the neutron spectral function in neutron matter for the Av18 interaction. The spectral function for densities ranging from $\rho = 0.04$ fm^{-3} to $\rho = 0.32$ fm^{-3} at a fixed temperature of $T = 5$ MeV is shown in the left panels for three momenta: $k = 0$ (top panel), $k = k_F$ (middle panel) and

$k = 2k_F$ (bottom panel), where k_F corresponds to the Fermi momentum associated with each density. The right panels show the results for a fixed density, $\rho = 0.16$ fm^{-3}, and temperatures from T= 5 to 20 MeV. The spectral functions are characterized by the presence of an important quasi-particle peak, which contains roughly $70\% - 80\%$ of the total strength for all momenta. The location of this peak is defined by the quasi-particle energy which is the solution of the equation:

$$\varepsilon_{qp}(k) = \frac{\hbar^2 k^2}{2m} + Re\Sigma(k, \varepsilon_{qp}(k)) \,. \tag{11}$$

With increasing density, the quasi-particle peak at zero momentum shifts to lower energies with respect to the chemical potential, *i.e.* neutrons at low momenta are more bound at higher densities. The situation is the opposite for high momenta ($k \sim 2k_F$), where the peak shifts to higher energies when density increases. At the Fermi surface, $k = k_F$ the quasi-particle peak is approximately centered around the chemical potential and its width decreases as ρ increases. At zero temperature and in the absence of pairing correlations, the spectral function would actually have a delta-like quasi-particle peak, whose strength defines the discontinuity of the momentum distribution at the Fermi surface at zero temperature. The strength in the tails of the spectral functions, both for large removal ($\omega << \mu$) and large addition ($\omega >> \mu$) energies, increases with density. These off-shell components of the spectral function are populated mainly due to short-range correlations and therefore they increase when the mean separation distance between the neutrons decreases. The influence of the temperature on the spectral function is less pronounced. Both the position of the quasi-particle peak and the strength at low and high energies are almost unaffected by changes in temperature. The only region that is slightly modified corresponds to $\omega \sim \mu$, which is particularly sensitive to variations in phase space.

Using Eq. (6) we can calculate the momentum distributions. Fig. 2 shows $n(k)$ of symmetric (upper panels) and neutron (lower panels) matter for the Av18 interaction at $T = 5$ MeV for four different densities. In the left panels $n(k)$ is displayed as a function of the ratio k/k_F. At a constant T, an increase in density leads to a more degenerate system. Consequently, the high density results have a more zero-temperature-like structure, with an almost constant depletion below k_F and a substantial jump in $n(k)$ at $k = k_F$. The occupation $n(0) \sim 0.85$ at $\rho = 0.16$ fm^{-3} characterizes the depletion of the momentum states in nuclear matter below the Fermi momentum. In contrast, at low densities, the momentum distribution is modulated by temperature at all momenta. One can also observe that one major density effect is the redistribution of strength in the region close to the Fermi surface. The high momentum components are shown in the right panels of the figure on a logarithmic scale for momenta ranging between 500 and 1500 MeV. In both symmetric and neutron matter, the high-density results lead to a larger population of high-momentum states.

One way to learn on the effects of hh propagation on the energetics of the system is to compare the quasi-particle peak (Eq.(11)) obtained in the SCGF approach that includes the effects of hh propagation with the one calculated within the BHF approach that accounts only for pp states. In Fig. 3, we compare the real part of the on-shell self-energy, $Re\Sigma(k, \varepsilon_{qp}(k))$, for both approaches at densities $\rho = 0.08$, 0.16, and 0.24 fm^{-3} (left, middle and right panels, respectively) and temperatures $T = 5$ MeV (solid lines)

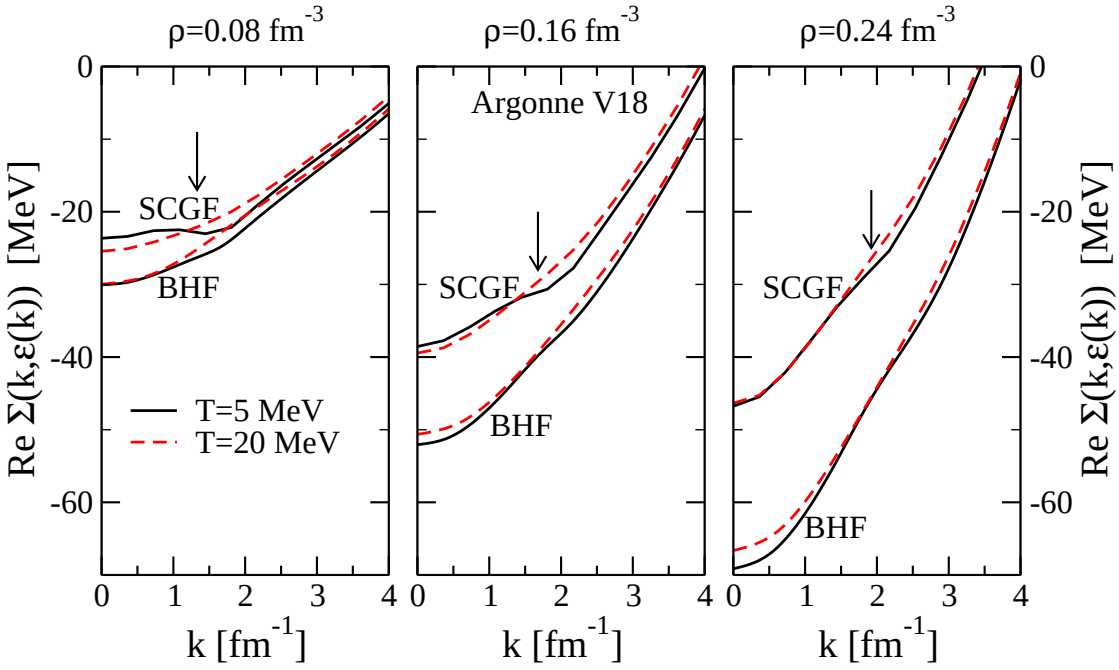

FIGURE 3. Comparison between the real part of the on-shell self-energy for SCGF and BHF approximations at $T = 5$ MeV (solid lines) and $T = 20$ MeV (dashed lines), calculated for neutron matter using the Av18 interaction. The three panels correspond to densities 0.08 fm^{-3} (left), 0.16 fm^{-3} (middle), and 0.24 fm^{-3} (right). The arrows show the associated Fermi momenta.

and $T = 20$ MeV (dashed lines). The results reported correspond to the Av18 potential, but similar conclusions are reached with the CDBonn. For all cases, the SCGF spectra are more repulsive than the BHF ones at all momenta. The effect of hh propagation on the on-shell self-energy is therefore of repulsive nature. This effect is larger at low momenta and the effect increases with density. Therefore, one also expects an overall repulsive effect of the propagation of holes when calculating the total energy.

THERMODYNAMICAL PROPERTIES OF NUCLEAR MATTER

For a complete thermodynamical description of the system, one should compute the free energy, $F = E - TS$. Therefore, one needs a suitable method to compute the entropy. It turns out that the knowledge of the single-particle propagator allows for the construction of the grand-potential, Ω, in the framework of the Luttinger-Ward formalism [21, 22]. From the grand-potential , one can obtain the entropy through the thermodynamical relation $S = -\frac{\partial \Omega}{\partial T}\,|_{\mu}$. To this end, it is convenient to split the entropy in two terms, $S = S^{DQ} + S'$. The first term is the so-called dynamical quasi-particle entropy:

$$S^{DQ} = \nu \int \frac{d^3k}{(2\pi)^3} \int_{-\infty}^{\infty} \frac{d\omega}{2\pi} \sigma(\omega) B(k,\omega)\,, \tag{12}$$

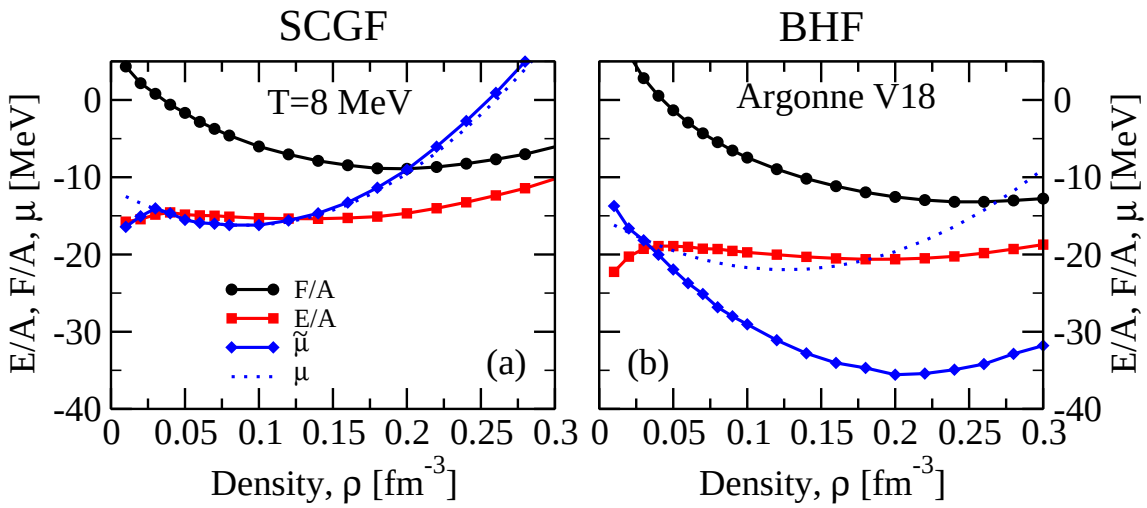

FIGURE 4. Energy per particle (circles), free energy per particle (squares) and chemical potential derived from the density sum-rule ($\bar{\mu}$)(diamonds) or from the free-energy through the thermodynamical definition (μ) (dotted line).

formed by the convolution of a statistical factor, $\sigma(\omega) = -f(\omega)\ln f(\omega) - [1 - f(\omega)]\ln[1 - f(\omega)]$, times a certain spectral function $B(k,\omega)$, closely related to the self-energy and the single-particle spectral function:

$$B(k,\omega) = A(k,\omega)\left[1 - \frac{\partial Re\Sigma(k,\omega)}{\partial\omega}\right] - 2\frac{\partial ReG(k,\omega)}{\partial\omega} Im\Sigma(k,\omega)\,. \qquad (13)$$

S^{DQ} takes into account the correlations of the dressed particles in the medium and includes finite width effects. In the following, we shall make the assumption that the second term of the entropy, S', is negligible. This approximation leads to thermodynamical consistent results [13], supporting the assumption that the contribution of S' is small in the range of density and temperature explored.

The knowledge of the entropy allows for the calculation of the free energy and a complete thermodynamical description of the system. The free energy per particle (squares) together with the energy per particle (circles) and the chemical potential (diamonds) are shown in Fig. 4 as a function of the density, at $T = 8$ MeV for the Av18 interaction. The left panel contains the results of SCGF and the right panel displays the BHF ones. As mentioned above, the hole-hole propagation, which is included in the SCGF but not in the BHF approach, yields a repulsive contribution to the energy. Since this repulsive contribution tends to increase with the nuclear density, one obtains a smaller saturation density in the SCGF than in the BHF approach. A similar effect is also observed for the free energy per particle, since the entropies calculated in both approaches are quite close to each other. The chemical potential, which is also shown in the figure, is useful to study the thermodynamical consistency of a many-body method. The chemical potential can be calculated from the density sum-rule (Eq. (8)), $\bar{\mu}$ (diamonds), or alternatively it can also be computed as the derivative of the free energy with respect to the number of nucleons at constant temperature, $\mu = \partial F/\partial N\,|_T$ (dotted lines). If the method is thermo-

dynamically consistent, the equality $\bar{\mu} = \mu$ holds. The differences between $\bar{\mu}$ and μ for the BHF approach can be larger than 15 MeV, showing its lack of consistency. Note that, in particular, the Hugenholtz-van Hove theorem is violated, *i.e.* $\bar{\mu}$ does not coincide with F/N at its minimum. The SCGF results, however, fulfil thermodynamical consistency. The next natural improvement of this approach in order to have a fully competitive and quantitative description of nuclear systems is the inclusion of three-body forces which play an important role at medium and high densities. Work along these lines is presently in progress.

ACKNOWLEDGMENTS

This work has been supported by grant No. FIS2008-01661 (Spain), by grant No. 2009SGR1289 from Generalitat de Catalunya, by the U.S. National Science Foundation under grants PHY-0652900 and PHY-0968941. A. Rios has been supported by a Marie Curie fellowship within the 7^{th} framework programme, STFC grant ST/F012012.

REFERENCES

1. H. Müther, and A. Polls, *Prog. Part. Nucl. Phys.* **45**, 243 (2000).
2. R. Machleidt, F. Samarruca and Y. Song, *Phys. Rev. C***53**,R1438 (1996).
3. R. B. Wiringa, V. G. J. Stocks and R. Schiavilla, *Phys. Rev. C***51** ,38 (1995).
4. A. Akmal and V. R. Pandharipande, *Phys. Rev. C***56**, 2261 (1997).
5. S. Fantoni, in *Introduction to Modern Methods of Quantum Many-Body Theory and their applications*, edited by A. Fabrocini, S. Fantoni, and E. Krotscheck, World Scientific, Singapore, 2002, pp. 379.
6. J. Carlson, J. Morales, V. R. Pandharipande, and D. G. Ravenhall, *Phys. Rev.* **68**, 025802 (2003).
7. S. Gandolfi, A. Y. Illarionov, S. Fantoni, F. Pederiva and K. E. Schmidt, *Phys. Rev. Lett.* **101**, 132501 (2008).
8. B. D. Day, *Rev. Mod. Phys.* **39**, 719 (1967).
9. M. Baldo and G. F. Burgio, in *Microscopic Theory of Nuclear Euqation of State and Neutron Star Structure*, edited by D. Blaschke, N. K. Glendenning, and A. Sedrakian, Springer Verlag, Heidelberg, 2001.
10. W. H. Dickhoff and C. Barbieri, *Prog. Part. Nucl. Phys.* **52**, 377 (2004).
11. Y. Dewulf, W. H. Dickhoff, D. Van Neck, E. R. Stoddard, and M. Waroquier, *Phys. Rev. Lett.* **90**, 152501 (2003).
12. T. Frick, H. Müther, A. Rios, A. Polls, and A. Ramos, *Phys. Rev. C***71**, 014313 (2005).
13. A. Rios, A. Polls, A. Ramos, and H. Müther, *Phys. Rev. C***74**, 054317 (2006).
14. A. Rios, A. Polls, A. Ramos, and H. Müther, *Phys. Rev. C***78**, 044314 (2008).
15. A. Rios, A. Polls, and I. Vidana, *Phys. Rev. C***79**, 025802 (2009).
16. A. Rios, A. Polls, and W. H. Dickhoff, *Phys. Rev. C***79**, 064308 (2009).
17. V. Somà and P. Bozek, *Phys. Rev. C***80**, 025803 (2009).
18. H. Müther and W. H. Dickhoff, *Phys. Rev. C***72**, 054313 (2005).
19. D. Rohe *et al. Phys. Rev. Lett.* **93**, 182501 (2004).
20. L. Lapikas *et al. Phys. Rev. Lett.* , to be submitted.
21. J. M. Luttinger and J. C. Ward, *Phys. Rev.*, **118**, 1417 (1960).
22. G. M. Carneiro and C. J. Pethick, *Phys. Rev. B* **11**, 1106 (1975).